



OPEN

SUBJECT AREAS:

NANOCAVITIES

NANOPHOTONICS AND
PLASMONICSReceived
26 November 2013Accepted
2 April 2014Published
2 May 2014

Correspondence and requests for materials should be addressed to L.Z. (zhouli@whu.edu.cn); Q.H.X. (Qihua@ntu.edu.sg) or Q.-Q.W. (qqwang@whu.edu.cn)

* These authors contributed equally to this work.

Manipulating Nonlinear Emission and Cooperative Effect of CdSe/ZnS Quantum Dots by Coupling to a Silver Nanorod Complex Cavity

Fan Nan^{1*}, Zi-Qiang Cheng^{1*}, Ya-Lan Wang¹, Qing Zhang², Li Zhou^{1,2}, Zhong-Jian Yang³, Yu-Ting Zhong¹, Shan Liang¹, Qihua Xiong^{2,4} & Qu-Quan Wang¹

¹Department of Physics, Wuhan University, Wuhan 430072, P. R. China, ²Division of Physics and Applied Physics, School of Physical and Mathematical Sciences, Nanyang Technological University, Singapore 637371, ³Beijing Computational Science Research Center, Beijing 100084, P. R. China, ⁴NOVITAS, Nanoelectronics Centre of Excellence, School of Electrical and Electronic Engineering, Nanyang Technological University, Singapore 639798.

Colloidal semiconductor quantum dots have three-dimensional confined excitons with large optical oscillator strength and gain. The surface plasmons of metallic nanostructures offer an efficient tool to enhance exciton-exciton coupling and excitation energy transfer at appropriate geometric arrangement. Here, we report plasmon-mediated cooperative emissions of approximately one monolayer of ensemble CdSe/ZnS quantum dots coupled with silver nanorod complex cavities at room temperature. Power-dependent spectral shifting, narrowing, modulation, and amplification are demonstrated by adjusting longitudinal surface plasmon resonance of silver nanorods, reflectivity and phase shift of silver nanostructured film, and mode spacing of the complex cavity. The underlying physical mechanism of the nonlinear excitation energy transfer and nonlinear emissions are further investigated and discussed by using time-resolved photoluminescence and finite-difference time-domain numerical simulations. Our results suggest effective strategies to design active plasmonic complex cavities for cooperative emission nanodevices based on semiconductor quantum dots.

Surface plasmon resonance (SPR) in metallic nanostructures, which is the collective oscillation of electrons in a metal surface excited by incident light, offers a powerful tool for field enhancement, localization, and confinement on the nanoscale^{1,2}. In addition, SPR has spurred the development of various kinds of active and passive plasmonic nanodevices for diverse applications, such as the use in bio-sensors, chemical catalysis, super-resolution imaging, and quantum information processing^{3,4}. Especially, diverse metallic nanostructures such as films, nanowires and nanoparticles have been integrated with gain materials in the active devices to overcompensate the SPR damping and radiative losses^{5–20}, resulting in the achievement of several important milestones for plasmonic amplification and lasing^{21–25}. For instance, the stimulated emission of surface plasmons has been first observed at the interface between a silver film and a dye solution with Kretschmann configurations²¹; surface plasmon amplification by the stimulated emission of radiation (SPASER) has been realised in gold nanoparticles coated with dye molecules²²; and plasmonic nanolasers at a deep subwavelength scale have been demonstrated in a silver film supporting a CdS nanowire and a GaN nanorod, respectively^{23–25}. These prominent achievements open the door for a new kind of nanophotonic source based on the coherent coupling of a surface plasmon and the gain materials.

Two-dimensional vertical metal nanorod arrays have tunable longitudinal and transverse plasmon resonances (abbreviated by L-SPRs and T-SPRs, respectively) via the free electrons near the metal surface oscillating along or perpendicular to the long axis of the nanorods. Strong coupling between the nearby metal nanorods induces the generation of standing waves in the plasmonic cavities and the formation of epsilon-near-zero plasmonic metamaterials^{26,27}. Resonant transmission and reflection plasmon modes induced by T-SPRs are first observed in Au nanorod arrays with a far-field excitation²⁸. The optical nanoemitters can be efficiently coupled to metal nanorods with a large Purcell factor²⁹. In addition, they can generate subwavelength images of those nanoemitters at the opposite ends of the nanorods due to a focusing effect, while the radiative energy transfer exhibits a higher

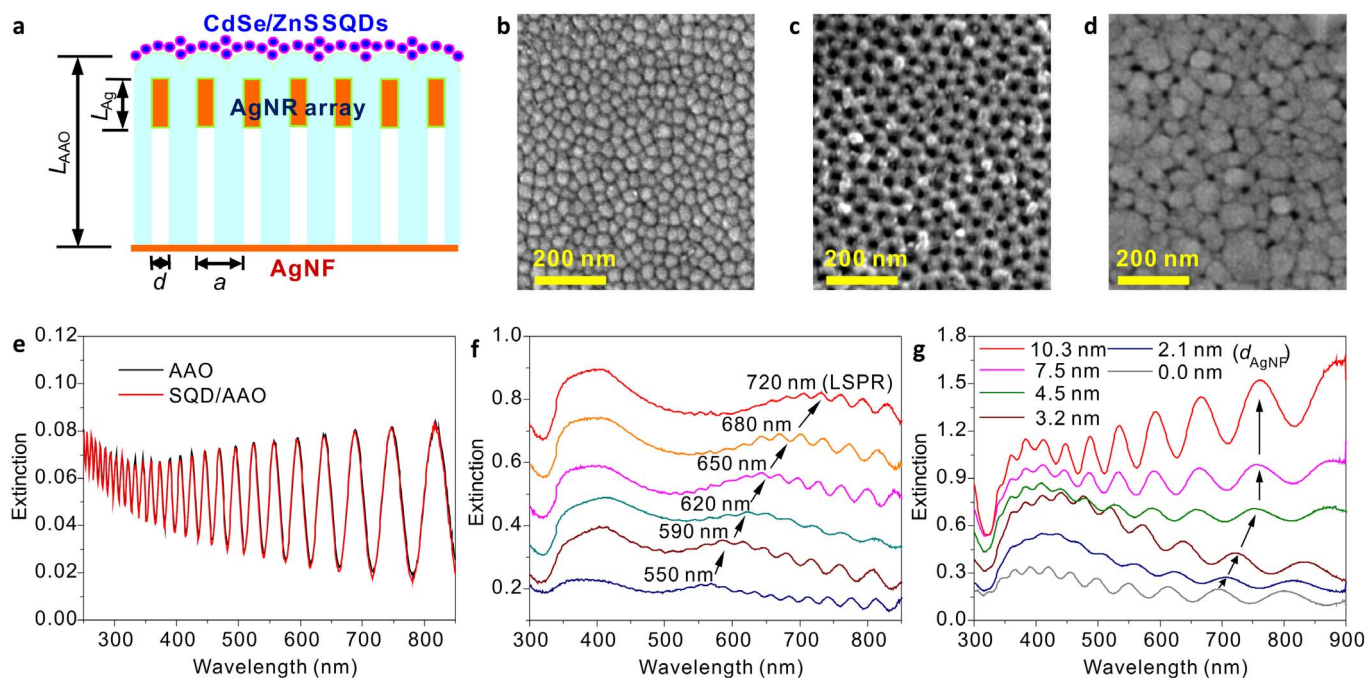


Figure 1 | Nanostructure and optical responses of the AgNR:AAO/AgNF complex cavity. (a) Illustration of nanostructure of the SQR/AgNR:AAO/AgNF. (b) Top-view of SEM images of the complex cavity. (c,d) Bottom view of SEM images of the complex cavity before and after deposition of AgNF. (e) Extinction spectra of the AAO cavity with and without spin-coated SQRs (incident angle $\theta_{in} = 0^\circ$). (f) Extinction spectra of the AgNR:AAO cavities with $\lambda_{L-SPR} = 550, 590, 620, 650, 680$ and 720 nm ($\theta_{in} \approx 80^\circ$). (g) Extinction spectra of AgNR:AAO/AgNF cavities with $d_{AgNF} = 0.0, 2.1, 3.2, 4.5, 7.5,$ and 10.3 nm ($\theta_{in} = 0^\circ$).

efficiency and improved directionality^{30–32}. These behaviors demonstrate the advantages of metal nanorod arrays as a plasmonic cavity for both far- and near-field optical sources.

Semiconductor quantum dots (SQDs), with size tunability and strong quantum confinement, offer the potential for tunable and scalable single-photon sources as well as cooperative emission devices. Ensemble SQDs have intrinsic advantages as gain media owing to their efficient excitation energy transfer and high quantum yield^{33,34}. Several forms of cooperative emission effects (including superradiance, amplified spontaneous emission (ASE), and stimulated emissions) from ensemble SQDs have been reported^{35–45}. Experimental evidence for a long-range electromagnetic interaction of superradiance has been observed by measurements of lifetime of laterally arranged SQDs³⁵. ASE and stimulated emissions from SQDs have been demonstrated with a variety of photonic structures, such as microspheres^{36–38}, microrings³⁹, cylindrical microcavities⁴⁰, waveguides and close-packed thick films^{41–45}. SQDs also have unique advantages for interacting with surface plasmons^{46–51}, and single SQDs interacting with a silver nanowire lead to the first observations of single plasmons⁴⁶. The plasmon excitation of CdSe SQDs demonstrates all-optical plasmonic modulation⁴⁷. ASE processes of PbS SQDs doped in PMMA on gold film lead to an increased plasmon propagation length and narrowed output spectrum⁴⁸. Spectral narrowing and shifting of the CdSe/ZnS SQDs coupled to Ag nanoisland films was also reported⁵¹. However, the cooperative emissions of ensemble SQDs assisted by plasmon cavities leaves a plenty of opportunity for investigation.

In this paper, we study the optical responses of plasmonic complex cavities consisting of a silver nanorod (AgNR) array electrochemically deposited in an anodic aluminum oxide (AAO) template nanopores, and a silver nanostructured film (AgNF) deposited on the back side of the template (AgNR:AAO/AgNF). We investigate the power-dependent cooperative emission behaviors of approximately one monolayer of CdSe/ZnS SQDs coupled with AgNR:AAO/AgNF complex cavities, and demonstrate the tunable spectral modulation

and amplification in the nanosystems by adjusting L-SPR peak of AgNRs, thickness of AgNF, and cavity-mode spacing. The corresponding physical mechanisms including power-dependent excitation energy transfer and cooperative radiances are discussed in detail by measurement and analysis of power-dependent photoluminescence (PL) lifetime.

Results

Nanostructures and optical responses of the AgNR:AAO/AgNF complex cavity. Our plasmon-exciton nanosystem consists of CdSe/ZnS SQDs coupled with an AgNR:AAO/AgNF complex cavity, as illustrated in Figure 1a, where AgNR array functions as a plasmonic cavity and AAO with a AgNF acts as a Fabry-Pérot cavity. The CdSe/ZnS SQDs are spin-coated onto the surface of the alumina barrier layer, which acts as a spacer between the SQDs and AgNRs. The thickness of the barrier layer is adjusted to be ~ 15 nm, within the optimal spacer distance for efficient coupling between SQDs and AgNRs and depressing fluorescence quenching. The thickness of the coated SQDs is approximately one monolayer (Figure S2). The arrayed AgNRs have an average diameter $d \approx 18$ nm and a period $a \approx 50$ nm (Figure 1b and 1c). The AgNF with thickness of 10 nm exhibits a porous nature with the voids less than 5 nm (Figure 1d and Figure S3).

The extinction spectra of the empty AAO template with and without CdSe/ZnS SQDs recorded by a normal incident light source are presented in Figure 1e. The periodic oscillations in the extinction spectra are due to the interference of the incident light reflected at the two surfaces of the AAO template with a high refractive index, and the minimal and maximal extinction correspond to the resonant transmittance and resonant reflection modes of these Fabry-Pérot cavities, respectively. After the spin-coating of CdSe/ZnS SQDs on the surface of the barrier layer of the empty AAO template, the extinction is increased ~ 0.005 in the violet region. The central PL wavelength ($\lambda_{SQD,0}$) of individual SQDs without interactions is ~ 588 nm and the full width at half maximum (FWHM) $\Delta\lambda_{SQD,0}$ is



~ 31.5 nm (112 meV). The cavity-mode spacing Δv_{cav} is adjusted in the range of $0.5\text{--}1.8\Delta v_{\text{SQD},0}$ for the purpose of observations of multi-mode and few-mode oscillations and amplifications by controlling the optical thickness of the cavities.

The L-SPR wavelengths of the AgNRs embedded in the AAO cavities are tuned by adjusting the electrochemical growth time of the nanorods. The tuning is confirmed by recording the extinction spectrum using a *p*-polarized light source with an incident angle of $\theta_{\text{in}} \approx 80^\circ$ (Figure 1f). The oblique incidence with *p*-polarization could excite the L-SPR in AgNRs. The central L-SPR peaks ($\lambda_{\text{L-SPR}}$) of the AgNRs are tuned to being resonant, near-resonant, and off-resonant with the emission peak $\lambda_{\text{SQD},0}$ (~ 590 nm) of the CdSe/ZnS SQDs. Moreover, the interference oscillation amplitude and phase of the complex cavity are tuned by adjusting thickness of the sputtered AgNFs as shown in Figure 1g, where the oscillation amplitude is significantly increased and the interference phase shifts more than π when $d_{\text{AgNF}} > 7.5$ nm.

Tunable spectral modulations of the ensemble SQDs coupled with the complex cavity. We first investigate the spectral modulation of the SQDs/cavity nano-systems by increasing the thickness of AgNF of the cavity and the excitation power. Figure 2a displays normalized PL spectra of the SQDs coupled to six AgNR:AAO/AgNF complex cavities with various AgNF thickness $d_{\text{AgNF}} = 0.0, 2.1, 4.5, 7.5, 10.3,$ and 13.5 nm. In which, the PL spectra are taken in reflective geometry and the excitation power is fixed at ~ 0.5 mW. As d_{AgNF} increases to 13.5 nm, the phase of the modulated PL spectra by cavity modes is shifted and the oscillation amplitude is significantly increased as well as the extinction spectra. The reflectivity of the back surface of the cavity increases from ~ 0.03 to ~ 0.36 and the phase shift measured by extinction spectrum reaches $\sim 3\pi/2$ (Figure S4a and S4b). The phase shift of AgNF induces variation of PL resonance wavelength (Figure 2a), while the enhanced reflectivity leads to an increase of PL modulation factor $\gamma = (I_{\text{PL,max}} - I_{\text{PL,min}})/I_{\text{PL,max}}$ from 0.26 to 0.87 (Figure 2c). The reflectivity of the back

surface of the cavity could be further enhanced by increasing the thickness of AgNF.

Interestingly, the spectral modulation of the SQDs coupled to the AgNR:AAO cavity (without AgNF) is significantly enhanced by increasing the excitation power (Figure 2b). The grey dashed lines in Figure 2b label the positions of five cavity modes and the peak positions are obtained from the multi-peak fitting of experimental spectra (Figure S9b). As the excitation power increases from 0.01 to 10 mW, the modulating factor γ increases from 0.22 to 0.37 (Figure 2d). Meanwhile, the emission peak around 586 nm has a slight blue-shift (~ 2.2 nm), and the central wavelength of the PL envelope shifts from 586 to 596 nm (Figure S4c). The power-dependent blue-shift of the PL peak is also observed in the emissions of the cavity itself (Figure S5). The power-dependent red-shift of the PL envelope is observed in both transmittance and reflection geometry (Figure S6), this is different from the dye molecules in the thick strongly-scattering media⁵², where the spectra show power-dependent red- and blue-shifts in reflection and transmission geometry. These blue- and red-shifts are hardly to be observed at the SQDs on empty AAO and quartz substrates (Figure S7).

The spectral modulating factor can be approximately expressed as (see details in SI),

$$\gamma = \frac{4kr_2e^G}{(1+kr_2e^G)^2}, \quad (1)$$

where r_2 is reflective coefficient of the back surface of the cavity, and k is coupling factor of the SQDs with the cavity. e^G represents the variations of amplitude of the PL electromagnetic field travel a circle in the cavity, which includes all factors, such as gain, propagation loss, and excitation energy transfer and relaxation from the higher level(s) to the lower one(s).

The observed spectral modulation shown in Figure 2 can qualitatively explained by using Equation 1. For the samples SQD/AgNR:AAO/AgNF with fixed excitation power and variable thickness of the AgNF, the increased reflective coefficient by the AgNF

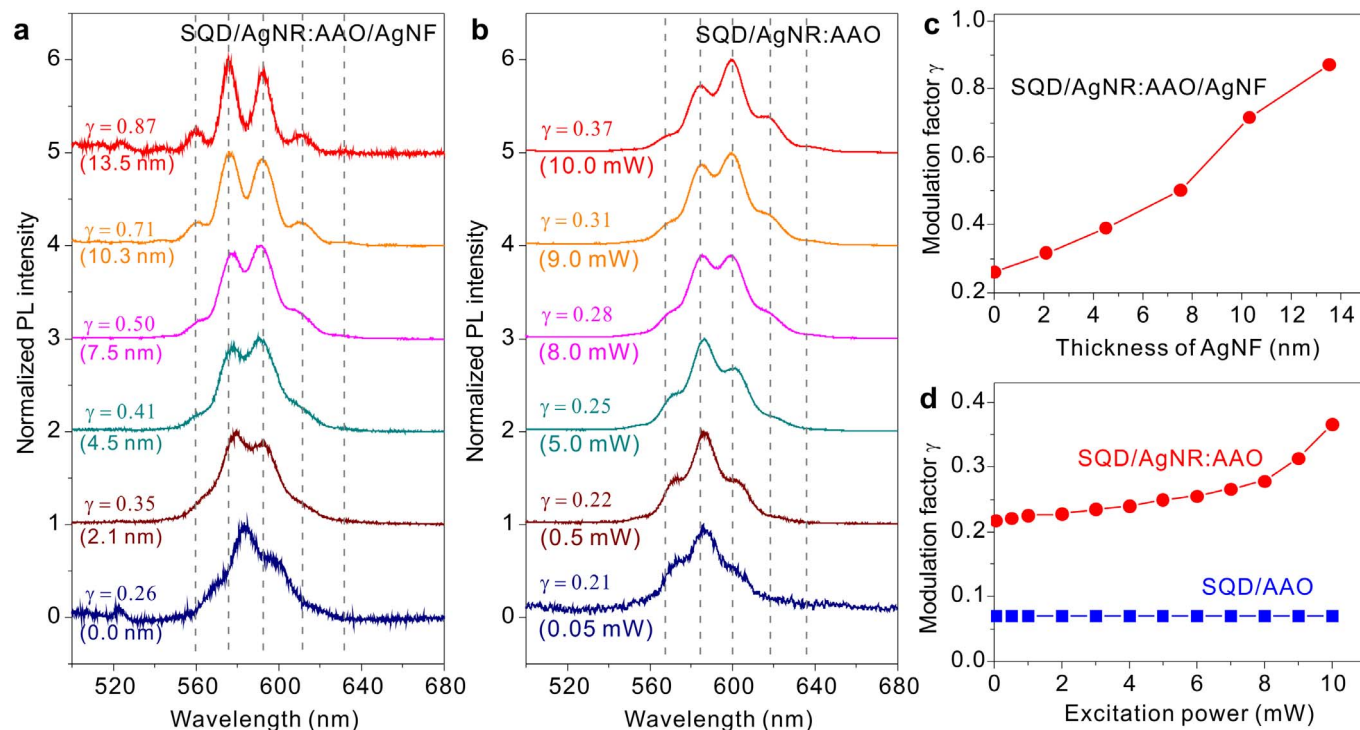


Figure 2 | Tunable spectral modulations of the ensemble SQDs coupled with complex cavities. (a) Normalized modulating PL spectra of the sample SQD/AgNR:AAO/AgNF with different thickness of AgNFs ($P = 0.5$ mW). (b) Normalized modulating PL spectra of the sample SQD/AgNR:AAO with different excitation power P . (c,d) Spectral modulating factor γ as a function of d_{AgNF} and P . γ increases with d_{AgNF} as well as P .

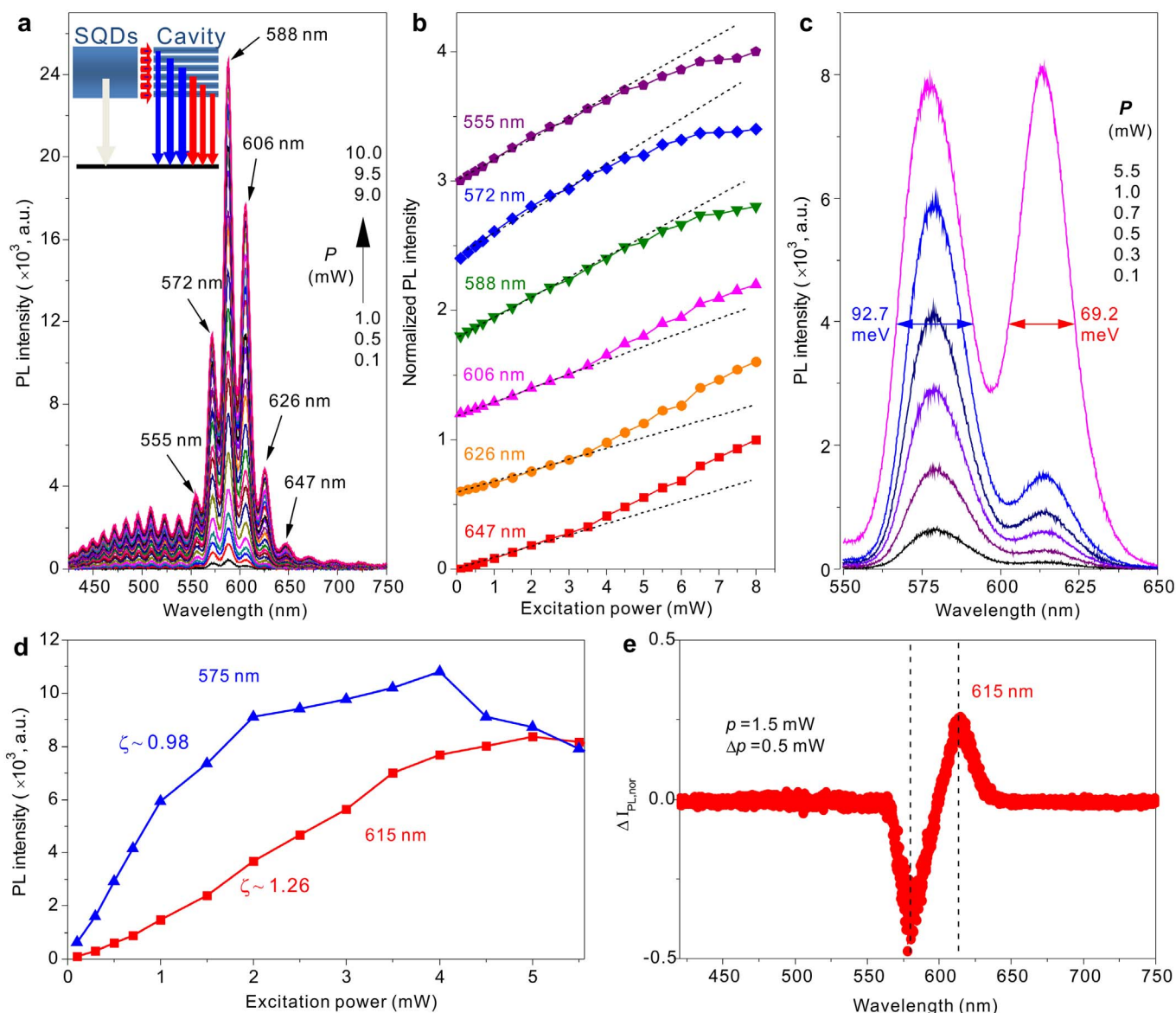


Figure 3 | Power-dependent multi-mode and few-mode oscillations and amplifications of the SQD/AgNR:AAO/AgNF. (a) Power-dependent PL spectra with multi-mode oscillations ($\Delta v_{\text{cav}} \approx 0.54\Delta v_{\text{SQD},0}$, $\bar{\lambda}_{\text{L-SPR}} \approx 660$ nm, and $d_{\text{AgNF}} = 10.3$ nm). (b) Power-dependences of the normalized peak PL intensity of six cavity modes at the emission wavelengths of 555, 572, 588, 606, 626, and 647 nm. (c) Power-dependent emission spectra with two-mode oscillations ($\Delta v_{\text{cav}} \approx 1.27\Delta v_{\text{SQD},0}$, $\bar{\lambda}_{\text{L-SPR}} \approx 610$ nm, $d_{\text{AgNF}} = 10.3$ nm). (d) Power dependences of the emission at 575 nm and 615 nm. (e) Differential normalized PL spectrum. The emissions around 575 nm are depressed and the emissions around 615 nm are amplified.

results in significant improvement of the modulating factor. For the samples SQD/AgNR:AAO without AgNF, the modulating factor γ is significantly improved as the excitation power increases, which indicates an equivalent nonlinear “gain” G in the nanosystem induced by the stronger excitation power.

Multi-mode oscillations and amplifications. The cavity-mode spacing Δv_{cav} is adjusted to about $0.54\Delta v_{\text{SQD},0}$ to observe the coupling of ensemble SQDs with multi-mode of the cavity. The power-dependent PL spectra of multi-mode oscillations for the SQDs/AgNR:AAO/AgNF cavity ($\Delta v_{\text{cav}} = 0.54\Delta v_{\text{SQD},0}$, $\bar{\lambda}_{\text{L-SPR}} = 660$ nm, $d_{\text{AgNF}} = 10.3$ nm) is shown in Figure 3a. The energy-level structures of the broaden emission band of the individual SQDs without interaction and the multi-mode of the cavity are illustrated in the inset. One can clearly see multi-mode oscillations of the cavity from the PL spectra. Owing to large reflectivity of the AgNF, the PL spectra of the SQDs around 590 nm are highly modulated. The emissions around 500 nm

from the AAO template itself are also modulated by the complex cavity itself. The spectral width (defined as the full width at half maximum) of the emission is directly extracted from the PL spectrum, which reaches as small as 11.5 nm (Figure S10a).

More interestingly, the SQDs populations coupled to the six modes of the complex cavity have different power dependences as shown in Figure 3b. The SQDs population on the cavity modes with wavelengths shorter and longer than $\lambda_{\text{SQD},0}$ is sublinearly and super-linearly dependent on the excitation power, respectively. The power dependence of the populations is qualitatively described by the slope index $\zeta = \log I / \log P$. As the excitation power increases, the slope index ζ decreases to 0.85, 0.65, and 0.78 for the three modes with wavelengths of 555, 572, and 588 nm, but increases to 1.25, 1.42, and 1.36 near threshold excitation power P_c for the three modes with wavelengths of 606, 626, and 647 nm (Figure S10b). This indicates that the emissions of the SQDs coupled to the three cavity modes with wavelengths longer than $\lambda_{\text{SQD},0}$ are nonlinearly amplified.

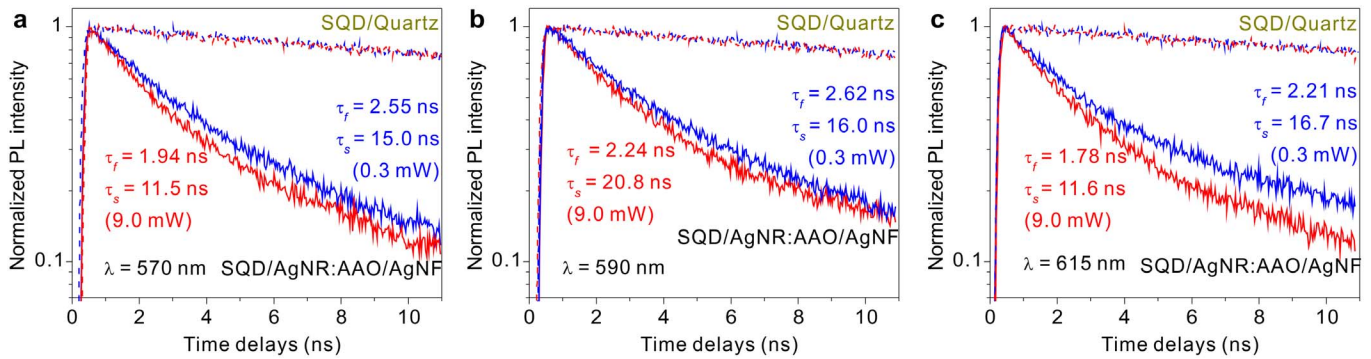


Figure 4 | Power-dependent emission dynamics of the ensemble SQDs coupled with a AgNR:AAO/AgNF complex cavity ($\Delta\nu_{\text{cav}} \approx 1.5\Delta\nu_{\text{SQD},0}$, $\bar{\lambda}_{\text{L-SPR}} \approx 610$ nm, $d_{\text{AgNF}} = 10.3$ nm). Time-resolved PL decay traces recorded at $\lambda_{\text{emi}} = 570$ nm (a), 590 nm (b), and 615 nm (c). The blue and red lines represent the results recorded with a weak and a strong excitation power ($P = 0.3$ and 9.0 mW). With weak excitation ($P = 0.3$ mW), $\tau_f = 2.55, 2.62,$ and 2.21 ns, $\tau_s = 15.0, 16.0,$ and 16.7 ns at $\lambda_{\text{emi}} = 570, 590$ and 615 nm. With strong excitation ($P = 9.0$ mW), $\tau_f = 1.94, 2.24,$ and 1.78 ns, $\tau_s = 11.5, 20.8,$ and 11.6 ns at $\lambda_{\text{emi}} = 570, 590$ and 615 nm.

Few-mode oscillations and amplifications. Then, the cavity-mode spacing $\Delta\nu_{\text{cav}}$ is increased to be comparable or larger than the spectral width $\Delta\nu_{\text{SQD},0}$ of the bare SQDs and the central L-SPR peak of the AgNRs is tuned to closed to $\lambda_{\text{SQD},0}$, which lead to oscillations and amplifications of a few modes. Figure 3c displays two-mode oscillations of SQD/AgNR:AAO/AgNF ($\Delta\nu_{\text{cav}} \approx 1.27\Delta\nu_{\text{SQD},0}$, $\bar{\lambda}_{\text{L-SPR}} \approx 610$ nm, $d_{\text{AgNF}} = 10.3$ nm), where only a single mode at 615 nm is amplified. Two emissions (centered at 575 nm and 615 nm) are well separated owing to large feedback field induced by AgNF on the back surface of the cavity. It's very interesting to compare the different power-dependence of these two emissions. (1) The PL intensity at 615 nm is amplified with slope index $\zeta = 1.26$, while the 575 nm emission becomes saturated and then decreases with the excitation power (Figure 3d). (2) The spectral width of the emissions at 615 nm decreases to 21.1 nm (69.2 meV) and the one at 575 nm increases to 24.7 nm (92.7 meV) as the excitation power increases (Figure 3c). The spectral width of 615 nm emission is 25.4% smaller than that of 575 nm emission at $P = 5.5$ mW. (3) The differential normalized PL intensity $\Delta I_{\text{PL,nor}}(\lambda) = I_{\text{PL}}(P + \Delta P, \lambda)/(P + \Delta P) - I_{\text{PL}}(P, \lambda)/P$ is positive around 615 nm owing to nonlinear amplifications (Figure 3e), but it is negative around 575 nm owing to nonlinear energy transfer and saturation. Notice that the nonlinear PL of the SQD/AAO:AgNR/AgNF sample with $\bar{\lambda}_{\text{L-SPR}} \approx 610$ nm has stronger saturable effect for the higher level and prominent spectral narrowing effect for the lower level comparing to those of the sample with $\bar{\lambda}_{\text{L-SPR}} \approx 660$ nm. The spectral narrowing and amplification at higher excitation power are not observed in the controlled samples without AgNRs (see Figure S8).

$\Delta I_{\text{PL,nor}}(\lambda)$ is approximately proportional to the differential “gain” $\Delta G = G(P + \Delta P, \lambda) - G(P, \lambda)$ (see Equations S4–S7 in SI). Therefore, a positive peak of $\Delta I_{\text{PL,nor}}(\lambda)$ around 615 nm indicates an increment of the “gain” ΔG at the stronger excitation, which is the origination of the emission amplifying as well as a power-dependent spectral narrowing. The peak position of this singly amplified emission is also tunable (in the range 605 ~ 620 nm) by adjusting mode-spacing and phase shift of the complex cavity.

Power-dependent emission dynamics. To reveal dynamic processes and physical mechanism of the nonlinear emissions of the ensemble SQDs coupled with a complex cavity, the PL lifetimes at different emission wavelength are measured with a weak and a strong excitation power by using time-resolved PL (TRPL) (Figure 4). The control sample SQD/quartz has a single PL decay process (dashed lines), which is almost independent on power. On the contrary, the TRPL decay trace of the sample SQD/Ag:AAO/AgNF ($\Delta\nu_{\text{cav}} \approx$

$1.5\Delta\nu_{\text{SQD},0}$, $\bar{\lambda}_{\text{L-SPR}} \approx 610$ nm, $d_{\text{AgNF}} = 10$ nm) is power-dependent and contains a fast and a slow process (solid lines), which is approximately reproduced by a two-component exponential function,

$$I(t) = A_f \exp\{-t/\tau_f\} + A_s \exp\{-t/\tau_s\}, \quad (2)$$

where τ_f (τ_s) and A_f (A_s) represent lifetime and weight factor of the fast (slow) process. As shown in Figure 4a–c, the TRPL recorded at three emission wavelengths ($\lambda_{\text{emi}} = 570, 590,$ and 615 nm) has different power-dependent behaviors.

i) For the emissions at the lower level ($\lambda_{\text{emi}} = 615$ nm $>$ $\lambda_{\text{SQD},0}$), the fast decay rate ($1/\tau_f$) increases from $1/2.21$ to $1/1.78$ ns $^{-1}$ as the excitation power increases from 0.3 to 9.0 mW, and the slow decay rate ($1/\tau_s$) also slightly increases. The rate increase of this level at strong excitation is larger than those of two other levels and is mainly attributed to power-enhanced radiative processes since the PL intensity is nonlinearly increases with the excitation power. ii) For the emissions at the higher level ($\lambda_{\text{emi}} = 570$ nm $<$ $\lambda_{\text{SQD},0}$), both fast and slow decay rates increase with the excitation power, but the PL intensity shows saturated-like behaviors, which indicates that the increase of decay rate of this level is mainly caused by power-enhanced nonradiative processes. iii) For the emissions around $\lambda_{\text{SQD},0}$ ($\lambda_{\text{emi}} = 590$ nm), the fast decay rate $1/\tau_f$ slightly increases from $1/2.62$ to $1/2.24$ ns $^{-1}$ but the slow decay rate decreases from $1/16.0$ to $1/20.8$ ns $^{-1}$ as the excitation power increases from 0.3 to 9.0 mW. This puzzled power-dependent dynamic behavior has also been observed in other SQD/Ag:AAO/AgNF samples with few-mode and implies a more complicated interaction processes in the nanosystem.

FDTD simulations for cooperative radiances. To further investigate enhancement of the radiative rate of the ensemble SQDs couple with an AgNRs complex cavity, we have performed the 3D-FDTD simulations of one and two radiative dipole sources on the top of AgNRs (Figure 5). Two-configurations of the two dipoles used in the FDTD calculations are shown in Figure 5a and 5e, respectively.

The radiative rate of two dipole sources (separated by 5 nm) in the middle of two AgNRs (Figure 5a) with a polarization along the short axis of the nanorods and with the same phase ($\Delta\varphi = 0$) are increased about 95% comparing to that of a single dipole coupled with the AgNRs, and the corresponding local fields of the two nanorods are significantly enhanced (Figure 5c and Figure S13). On the other hand, the radiance of the local field of two nanorods is almost totally depressed when the two dipoles are out of phase $\Delta\varphi = \pi$ (Figure 5d). These enhanced and depressed emissions are the superradiance and subradiance of two dipoles induced by surface plasmon of the AgNRs.

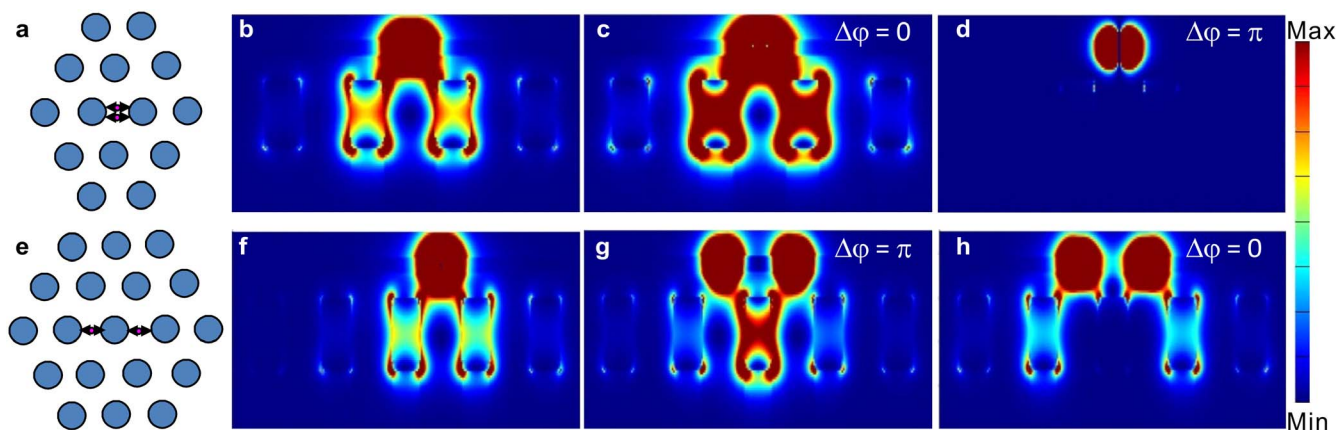


Figure 5 | Superradiance and subradiance of two dipole sources coupled with AgNRs. (a) and (e) Illustration of the positions and polarizations of two dipoles. (b–d) Local fields ($|E|^2$) of one and two dipoles coupled with AgNRs ($L_{\text{AgNR}} = 30$ nm, $\lambda = 600$ nm) by configuration shown in (a). (f–h) Local fields of one and two dipoles coupled with AgNRs ($L_{\text{AgNR}} = 32$ nm, $\lambda = 600$ nm) by configuration shown in (e). Enhanced radiances of two dipoles are demonstrated in (c) and (g), and the depressed radiances are demonstrated in (d) and (h).

Similar superradiance and subradiance are also demonstrated when the two dipoles located at the two sides of an AgNR (Figure 5e). The distance of two dipoles is as large as 40 nm, the local field around the central AgNR is enhanced $\sim 100\%$ by superradiance (when $\Delta\phi = \pi$, Figure 5g) and almost totally depressed by subradiance (when $\Delta\phi = 0$, Figure 5h). The probability of these cooperative emissions of the ensemble SQDs is larger than that of two SQDs and will increase with excitation power. Here it should be noted that, we use symmetric finite size rod arrays to calculate the cooperative behaviors. Although the structures are not periodic as that used in experiments, they are quite equivalent to investigate the cooperative effects between two QDs near a rod. Because the rods that are far away from the two QDs do not affect the coherent couplings. The near field distribution is also affected by the array parameters such as the rod distance, plasmon resonance of rods and the distance between QD and rods.

Discussion

Finally, we discuss relationships and underlying physical mechanisms for the nonlinear spectral shifting, narrowing, modulating, and amplification of the emissions from the ensemble SQDs coupled with plasmonic complex cavities based on the above observations and calculations. Three optical processes are probably involved in our nanosystem.

Nonradiative energy transfer to the lower-level mode(s). The observed saturated-like PL intensity and increased decay rate at the stronger excitation power at the higher level(s) (570 nm) are the strong evidence of the excitation energy transfer process from the higher to the lower level(s). Usually, the distance of efficient nonradiative energy transfer between SQDs is only few nanometers, but the surface plasmon of AgNRs largely extends this energy transfer distance to several tens of nanometers via exciton-plasmon-exciton resonant coupling^{53,54}.

Radiative energy transfer to the lower-level mode(s). The radiative emissions from AAO cavity itself and other SQDs with larger spatial distance are reabsorbed by the SQDs via radiative energy transfer process. The arrayed AgNRs strongly focus radiative field at the tops of the nanorods^{30–32}, therefore, the focused radiative energy are efficiently transferred to the SQDs nearby. This energy transfer process indicates that appropriate radiative emissions from the complex cavity itself increase the equivalent “gain” of the radiance at the lower level(s), but extremely strong PL of AgNRs around 590 nm will lead to spectral broadening of the SQDs^{55–57}.

Enhanced radiance of the lower-level mode(s). Both peak PL intensity and decay rate of the lower level(s) are increased and the corresponding spectral width is narrowed at stronger excitation, which indicates that the pumped population at the lower level radiates more efficient at stronger excitation power. The origin of these three spectral behaviors of nonlinear emissions has independently attributed to superradiance, stimulating emission and ASE, and we believe that the dominated process in our nanosystem is stimulating emission and superradiance enhanced by a vertical complex cavity rather than ASE assisted by a lateral waveguidance. The plasmon-enhanced superradiance of the ensemble SQDs could not be neglected since the threshold effect is very weak. The radiative rate of two or more SQDs (radiative dipoles) coupled with AgNRs with appropriate phase could be increased or depressed. The possibility of this cooperative processes is increased when more excitonic populations in the SQDs are pumped near the threshold regime. Additionally, a fast followed by a slow PL decay processes observed at stronger excitation is also coincided with the theoretical predictions of these cooperative emissions⁵⁸.

It is hard to distinguish the superradiance of the ensemble SQDs from the stimulated emissions with a soft-threshold, and the stimulating process increases the probability of in phase for two SQDs, which will then increase superradiance. Experimental studies on the super- and sub-radiances of the ensemble SQDs are relatively difficult than the cooperative emissions of rare-earth ions, where the cooperative energy transfer and radiation between two ion-dipoles with well-separated energy levels are relatively easy to be manipulated and observed by spectroscopy via efficient up- or down-converted luminescence^{59,60}. The multiexciton processes in SQDs could also lead to power-dependent nonlinear PL and emission dynamics^{61,62}. However, the lifetime of multiexciton processes is determined by the nonradiative Auger interaction and in picosecond scale. The experimental data with PL integrate time at microsecond scale and lifetime at nanosecond scale in this paper cannot be assigned to the multiexciton process. More experimental evidences (such as lifetime and photon-statistics) about the cooperative emissions of ensemble SQDs remain to be further studied.

In summary, we have demonstrated power-dependent spectral shifting, narrowing, modulation, and amplification of ensemble SQDs coupled to AgNR:AAO/AgNF complex cavities by tuning L-SPR of AgNRs, thickness of AgNF, and mode-spacing of the cavity. Amplified emissions of one, two, and three cavity-modes with narrowed spectrum and soft threshold of the ensemble SQDs are demonstrated. The nonlinear “gain” of the amplified emissions is analyzed from spectral modulation factor and differential PL



spectrum. Power-dependent enhancements of radiative and nonradiative rates are also observed at the lower and higher level(s). Superradiance and subradiance of two SQDs coupled to the AgNR array are demonstrated by FDTD simulations. Based on these measurements and analysis, we conclude that the observed nonlinear spectral behaviors are mainly attributed to stimulated emissions with a soft-threshold and superradiance of ensemble SQDs enhanced by the plasmonic complex cavity. Our findings offer a new strategy to design active plasmonic complex cavities and a powerful tool to manipulate cooperative emissions of the ensemble of optical radiative dipoles, leading to augmented properties of light emission diode devices or nanolasers.

Methods

Preparation of AgNR:AAO/AgNF complex cavities. The anodic aluminum oxide (AAO) templates were prepared by a two-step anodisation process. The polished aluminum sheets were exposed to a 0.3 M H₂SO₄ solution under constant voltage of 19 V in an electrochemical cell at a temperature of approximately 4°C. The alumina layer produced by the first anodization process was removed by wet chemical etching in a mixture of phosphoric acid (0.15 M) and chromic acid (0.60 M) at ~60°C, in order to obtain a fresh Al surface which is advantageous to achieve uniform AAO nanopore arrays. The AAO templates were anodized with a stepwise reduced potential from 19 V down to 13 V in H₂SO₄ solution to decrease the thickness of the AAO barrier layer. The AgNRs were grown in the nano-pores of AAO templates by alternating-current electrolysis (50 Hz, 7 V, AC) in an electrolyte containing AgNO₃ (0.03 M) and H₂SO₄ (0.03 M) with the underlying Al layer as an electrode and a Pt counter electrode. After dissolving the underlying Al substrate by using the mixture of HCl (1.2 M) and CuCl₂ (0.44 M) solution, the AgNR:AAO cavity was obtained. Then, the AgNFs were deposited onto the surface with nanopores of the AgNRs:AAO by using a magnetron sputtering (Quorum-K575X), forming an air gap between the AgNRs and the AgNF. The thickness of the deposited films was monitored by a quartz crystal.

Spin-coating CdSe/ZnS SQDs. Commercial carboxyl CdSe/ZnS core-shell quantum dots with central emission wavelengths of ~590 nm were purchased from Invitrogen Corporation. A 10 µL SQD suspensions was diluted by 490 µL purified water. A 13 µL droplet of the diluted QD suspensions was dropped onto the surface of the alumina barrier layer of the AgNR:AAO/AgNF cavity and rotated for 30 s at 1500 rpm.

Characterization of samples. The scanning electron microscopy (SEM) was performed using a FEG SEM Sirion 200 operated at an accelerating voltage of 25.0 kV. The transmission electron microscopy (TEM) was performed using a JEOL 2010HT operated at 100 kV. The TEM samples were prepared by dissolving the AAO template containing AgNRs in NaOH solution. The morphology of the back surface of the AAO templates with and without QDs was investigated by using atomic force microscopy (AFM, SPM-9500J3, Shimadzu). The absorption spectra were recorded by a UV-VIS-NIR spectrophotometer (Varian Cary 5000) by using a *p*-polarized source with an incident angle 80°, as shown in Figure S1a.

Optical experiments. The optical excitation source was a mode-locked Ti:sapphire laser (Mira 900, Coherent) with a pulse width of ~3 ps and a repetition rate of 76 MHz, and the excitation wavelength was tuned to 400 nm by using a second-harmonic generation system (HarmoniXX, APE GmbH). As shown in Figure S1b, a lens with a 150 mm focal length was used to focus the laser beam onto the sample, where the incident angle of the laser beam was ~80° and the area of the focus spot on the sample was approximately 6.7×10^{-4} mm². The PL signal from the samples was collected by a reflection measurement, filtered with two filters and recorded through a spectrometer (Spectrapro 2500i, Acton) with a liquid-nitrogen-cooled charge-coupled device (SPEC-10, Princeton). The time-resolved PL emission decay traces were recorded using a time-correlated single-photon counting system (PicoQuant GmbH).

Numerical simulations. The simulations were carried out by using the software FDTD Solutions 7.5. In the simulations, the refractive index of Ag rods is taken from Palik (*Handbook of Optical Constants of Solids*; Academic Press: New York, 1985). The index of the hole under each Ag rod is taken as 1, and the height of the holes is 500 nm. The Ag rod array has a period $a = 50$ nm and rod diameter $d = 20$ nm. The Ag rods with holes are placed in an AAO with refractive index 1.6. The quantum dots are taken as dipole emitters, and the layer height is 6 nm with index 2.5. The whole structure is placed in air with refractive index 1. Perfectly matched layer boundary conditions are used in the simulations.

1. Atwater, H. A. The promise of plasmonics. *Sci. Am.* **296**, 56–63 (2007).
2. Maier, S. A. *Plasmonics: Fundamentals and Applications*. (Springer, 2007).
3. Jin, Y. D. Engineering Plasmonic Gold Nanostructures and Metamaterials for Biosensing and Nanomedicine. *Adv. Mater.* **24**, 5153–5165 (2012).

4. Boriskina, S. V. & Reinhard, B. M. Spectrally and spatially configurable superlenses for optoplasmonic nanocircuits. *P. Natl. Acad. Sci. USA* **108**, 3147–3151 (2011).
5. Berini, P. & De Leon, I. Surface plasmon-polariton amplifiers and lasers. *Nat. Photonics* **6**, 16–24 (2012).
6. Noginov, M. A. *et al.* Stimulated emission of surface plasmon polaritons. *Phys. Rev. Lett.* **101**, 226806 (2008).
7. Ambati, M. *et al.* Observation of stimulated emission of surface plasmon polaritons. *Nano Lett.* **8**, 3998–4001 (2008).
8. Chen, Y. H., Li, J. F., Ren, M. L. & Li, Z. Y. Amplified Spontaneous Emission of Surface Plasmon Polaritons with Unusual Angle-Dependent Response. *Small* **8**, 1355–1359 (2012).
9. Liu, N. *et al.* Plasmonic Amplification with Ultra-High Optical Gain at Room Temperature. *Sci. Rep.* **3**, 1967 (2013).
10. Kitur, J. K., Podolskiy, V. A. & Noginov, M. A. Stimulated emission of surface plasmon polaritons in a microcylinder cavity. *Phys. Rev. Lett.* **106**, 183903 (2011).
11. Hill, M. T. *et al.* Lasing in metallic-coated nanocavities. *Nat. Photonics* **1**, 589–594 (2007).
12. Bosman, M. *et al.* Surface Plasmon Damping Quantified with an Electron Nanoprobe. *Sci. Rep.* **3**, 1312 (2013).
13. Nezhad, M. P. *et al.* Room-temperature subwavelength metallo-dielectric lasers. *Nat. Photonics* **4**, 395–399 (2010).
14. Thylén, L., Holmström, P., Bratkovsky, A., Li, J. J. & Wang, S. Y. Limits on Integration as determined by power dissipation and signal-to-noise ratio in loss-compensated photonic integrated circuits based on metal/quantum-dot materials. *IEEE J. Quant. Elect.* **46**, 518–524 (2010).
15. Banerjee, A., Li, R. & Grebel, H. Surface plasmon lasers with quantum dots as gain media. *Appl. Phys. Lett.* **95**, 251106 (2009).
16. Radko, I. P., Nielsen, M. G., Albrektson, O. & Bozhevolnyi, S. I. Stimulated emission of surface plasmon polaritons by lead-sulphide quantum dots at near infra-red wavelengths. *Opt. Express* **18**, 18633–18641 (2010).
17. De Leon, I. & Berini, P. Spontaneous emission in long-range surface plasmon-polariton amplifiers. *Phys. Rev. B* **83**, 081414(R) (2011).
18. Holmström, P., Thylén, L. & Bratkovsky, A. Composite metal/quantum-dot nanoparticle-array waveguides with compensated loss. *Appl. Phys. Lett.* **97**, 073110 (2010).
19. Noginov, M. A. *et al.* Enhancement of surface plasmons in an Ag aggregate by optical gain in a dielectric medium. *Opt. Lett.* **31**, 3022–3024 (2006).
20. Flynn, R. A. *et al.* A room-temperature semiconductor spaser operating near 1.5 µm. *Opt. Express* **19**, 8954–8961 (2011).
21. Seidel, J., Grafstrom, S. & Eng, L. Stimulated emission of surface plasmons at the interface between a silver film and an optically pumped dye solution. *Phys. Rev. Lett.* **94**, 177401 (2005).
22. Noginov, M. A. *et al.* Demonstration of a spaser-based nanolaser. *Nature* **460**, 1110–1112 (2009).
23. Oulton, R. F. *et al.* Plasmon lasers at deep subwavelength scale. *Nature* **461**, 629–632 (2009).
24. Ma, R. M., Oulton, R. F., Sorger, V. J., Bartal, G. & Zhang, X. A. Room-temperature sub-diffraction-limited plasmon laser by total internal reflection. *Nat. Mater.* **10**, 110–113 (2011).
25. Lu, Y. J. *et al.* Plasmonic nanolaser using epitaxially grown silver film. *Science* **337**, 450–453 (2012).
26. Evans, P. R. *et al.* Optical transmission properties and electric field distribution of interacting 2D silver nanorod Arrays. *Adv. Funct. Mater.* **18**, 1075–1079 (2008).
27. Pollard, R. J. *et al.* Optical Nonlocalities and additional waves in epsilon-near-zero metamaterials. *Phys. Rev. Lett.* **102**, 127405 (2009).
28. Lyvers, D. P., Moon, J. M., Kildishev, A. V., Shalaev, V. M. & Wei, A. Gold nanorod arrays as plasmonic cavity resonators. *ACS Nano* **2**, 2569–2576 (2008).
29. Chang, D. E., Sørensen, A. S., Hemmer, P. R. & Lukin, M. D. Quantum optics with surface plasmons. *Phys. Rev. Lett.* **97**, 053002 (2006).
30. Kawata, S., Ono, A. & Verma, P. Subwavelength colour imaging with a metallic nanolens. *Nat. Photonics* **2**, 438–442 (2008).
31. Ono, A., Kato, J. & Kawata, S. Subwavelength optical imaging through a metallic nanorod array. *Phys. Rev. Lett.* **95**, 267407 (2005).
32. Zhou, Z. K. *et al.* Plasmon-mediated radiative energy transfer across a silver nanowire array via resonant transmission and subwavelength imaging. *ACS Nano* **4**, 5003–5010 (2010).
33. Klimov, V. I. *et al.* Single-exciton optical gain in semiconductor nanocrystals. *Nature* **447**, 441–446 (2007).
34. Pavesi, L., Dal Negro, L., Mazzoleni, C., Franzo, G. & Priolo, F. Optical gain in silicon nanocrystals. *Nature* **408**, 440–444 (2000).
35. Scheibner, M. *et al.* Superradiance of quantum dots. *Nat. Physics* **3**, 106–110 (2007).
36. Chan, Y. *et al.* Blue semiconductor nanocrystal laser. *Appl. Phys. Lett.* **86**, 073102 (2005).
37. Snee, P. T., Chan, Y. H., Nocera, D. G. & Bawendi, M. G. Whispering-gallery-mode lasing from a semiconductor nanocrystal/microsphere resonator composite. *Adv. Mater.* **17**, 1131–1136 (2005).
38. Schäfer, J. *et al.* Quantum dot microdrop laser. *Nano Lett.* **8**, 1709–1712 (2008).
39. Malko, A. V. *et al.* From amplified spontaneous emission to microring lasing using nanocrystal quantum dot solids. *Appl. Phys. Lett.* **81**, 1303–1305 (2002).



40. Kazes, M., Lewis, D. Y., Ebenstein, Y., Mokari, T. & Banin, U. Lasing from semiconductor quantum rods in a cylindrical microcavity. *Adv. Mater.* **14**, 317–321 (2002).
41. Klimov, V. I. *et al.* Optical gain and stimulated emission in nanocrystal quantum dots. *Science* **290**, 314–317 (2000).
42. Schaller, R. D., Petruska, M. A. & Klimov, V. I. Tunable near-infrared optical gain and amplified spontaneous emission using PbSe nanocrystals. *J. Phys. Chem. B* **107**, 13765–13768 (2003).
43. Finlayson, C. E. *et al.* Amplified spontaneous emission in close-packed films of semiconductor nanocrystals using picosecond excitation. *Adv. Funct. Mater.* **12**, 537–540 (2002).
44. Jasieniak, J. J. *et al.* Highly efficient amplified stimulated emission from CdSe-CdS-ZnS quantum dot doped waveguides with two-photon infrared optical pumping. *Adv. Mater.* **20**, 69–73 (2008).
45. Zhang, C. *et al.* Two-photon-pumped lasing from colloidal nanocrystal quantum dots. *Opt. Lett.* **33**, 2437–2439 (2008).
46. Akimov, A. V. *et al.* Generation of single optical plasmons in metallic nanowires coupled to quantum dots. *Nature* **450**, 402–406 (2007).
47. Pacifici, D., Lezec, H. J. & Atwater, H. A. All-optical modulation by plasmonic excitation of CdSe quantum dots. *Nat. Photonics* **1**, 402–406 (2007).
48. Bolger, P. M. *et al.* Amplified spontaneous emission of surface plasmon polaritons and limitations on the increase of their propagation length. *Opt. Lett.* **35**, 1197–1199 (2010).
49. Mitsuishi, M., Morita, S., Tawa, K., Nishii, J. & Miyashita, T. Spontaneous emission control of CdSe/ZnS nanoparticle monolayer in polymer nanosheet waveguide assembled on a one-dimensional silver grating surface. *Langmuir* **28**, 2313–2317 (2012).
50. Briscoe, J. L., Jayasundara, N. & Cho, S. Y. Surface-plasmon-polariton assisted modification of spontaneous emission of colloidal quantum dots in metal nanostructures. *Appl. Phys. Lett.* **102**, 023113 (2013).
51. Soganci, I. M., Nizamoglu, S., Mutlugun, E., Akin, O. & Demir, H. V. Localized plasmon-engineered spontaneous emission of CdSe/ZnS nanocrystals closely-packed in the proximity of Ag nanoisland films for controlling emission linewidth, peak, and intensity. *Opt. Express* **15**, 14289–14298 (2007).
52. Totsuka, K., Talukder, M. A. I., Matsumoto, M. & Tomita, M. Excitation-power-dependent spectral shift in photoluminescence in dye molecules in strongly scattering optical media. *Phys. Rev. B* **59**, 50–53 (1999).
53. Govorov, A. O., Lee, J. & Kotov, N. A. Theory of plasmon-enhanced Förster energy transfer in optically excited semiconductor and metal nanoparticles. *Phys. Rev. B* **76**, 125308 (2007).
54. Durach, M., Rusina, A., Klimov, V. I. & Stockman, M. I. Nanoplasmonic renormalization and enhancement of Coulomb interactions. *New J. Phys.* **10**, 105011 (2008).
55. Boyd, G. T., Yu, Z. H. & Shen, Y. R. Photoinduced luminescence from the noble-metals and its enhancement on roughened surfaces. *Phys. Rev. B* **33**, 7923–7936 (1986).
56. Peyser, L. A., Vinson, A. E., Bartko, A. P. & Dickson, R. M. Photoactivated fluorescence from individual silver nanoclusters. *Science* **291**, 103–106 (2001).
57. Gangopadhyay, P. *et al.* Optical absorption and photoluminescence spectroscopy of the growth of silver nanoparticles. *Phys. Rev. Lett.* **94**, 047403 (2005).
58. Temnov, V. V. & Woggon, U. Superradiance and subradiance in an inhomogeneously broadened ensemble of two-level systems coupled to a low-Q cavity. *Phys. Rev. Lett.* **95**, 243602 (2005).
59. Kushida, T. Energy transfer and cooperative optical transitions in rare-earth doped inorganic materials. I. Transition probability calculation. *J. Phys. Soc. Jpn.* **34**, 1318–1326 (1973).
60. Kushida, T. Energy transfer and cooperative optical transitions in rare-earth doped inorganic materials. II. Comparison with Experiments. *J. Phys. Soc. Jpn.* **34**, 1327–1333 (1973).
61. Klimov, V. I., Mikhailovsky, A. A., McBranch, D. W., Leatherdale, C. A. & Bawendi, M. G. Quantization of multiparticle Auger rates in semiconductor quantum dots. *Science* **287**, 1101–1103 (2000).
62. Achermann, M. A., Hollingsworth, J. & Klimov, V. I. Multiexcitons confined within a subexcitonic volume: Spectroscopic and dynamical signatures of neutral and charged biexcitons in ultrasmall semiconductor nanocrystals. *Phys. Rev. B* **68**, 245302 (2003).

Acknowledgments

We gratefully thank Professors Wei Zhang and Xue-Hua Wang for helpful discussions, Dr. Zhong-Hua Hao for data analysis and manuscript preparation, Dr. Zhang-Kai Zhou, Mr. Ying Yu, Miss Qiu-Xia Zhu for sample preparations, and Dr. Xiao-Niu Peng for optical measurements. This work was supported in part by NSFC (11174229 and 61008043), National Basic Research Program of China (2011CB922200). Q.X. gratefully acknowledges Singapore National Research Foundation through a Fellowship grant (NRF-RF2009-06) and a Competitive Research Program (NRF-CRP-6-2010-2), Singapore Ministry of Education via a Tier2 grants (MOE2011-T2-2-051).

Author contributions

F.N. and Z.Q.C. contributed equally to this work. F.N. prepared the samples and performed optical experiments. Z.Q.C., Y.T.Z. and Y.L.W. prepared the AAO complex cavities and recorded absorption spectrum. S.L. and L.Z. performed the structural analysis. Z.J.Y. did FDTD simulations. Q.Z. and L.Z. helped with some of the experimental design and made significant contribution to data analysis and manuscript preparation and revision. Q.X., L.Z. and Q.Q.W. are responsible for the experimental design, data coordination, analysis and interpretation, writing, revising and finalization of the manuscript.

Additional information

Supplementary information accompanies this paper at <http://www.nature.com/scientificreports>

Competing financial interests: The authors declare no competing financial interests.

How to cite this article: Nan, F. *et al.* Manipulating Nonlinear Emission and Cooperative Effect of CdSe/ZnS Quantum Dots by Coupling to a Silver Nanorod Complex Cavity. *Sci. Rep.* **4**, 4839; DOI:10.1038/srep04839 (2014).



This work is licensed under a Creative Commons Attribution-NonCommercial-ShareAlike 3.0 Unported License. The images in this article are included in the article's Creative Commons license, unless indicated otherwise in the image credit; if the image is not included under the Creative Commons license, users will need to obtain permission from the license holder in order to reproduce the image. To view a copy of this license, visit <http://creativecommons.org/licenses/by-nc-sa/3.0/>